DEUTSCHES ELEKTRONEN – SYNCHROTRON

DESY 90-167
December 1990

Small-x Physics at LEP/LHC

J. Bartels and G. A. Schuler

II. Institut für Theoretische Physik, Universität Hamburg

ISSN 0418-9833

NOTKESTRASSE 85 · D-2000 HAMBURG 52

To be sure that your preprints are promptly included in the
HIGH ENERGY PHYSICS INDEX,
send them to the following (if possible by air mail):

DESY
Bibliothek
Notkestrasse 85
D-2000 Hamburg 52
Germany

DESY 90-167
December 1990

ISSN 0418-9833

Small-x Physics at LEP LHC[1]

J. Bartels and G. A. Schuler[2]

II. Institut für Theoretische Physik, Universität Hamburg, Germany

ABSTRACT

The small-x behavior of deep inelastic structure functions in QCD is discussed. After a brief review of theoretical ideas we describe numerical estimates which show that LEP/LHC will be extremely useful for distinguishing between "standard QCD" and "new" physics in the low-x region. We also discuss which measurements will be useful for unravelling the new features of small-x physics.

1 Theoretical Ideas

Deep Inelastic scattering of electrons on protons (DIS) provides the classical test of our parton picture of hadrons and, hence, of QCD at short distances. With the advent of HERA (anticipated for the summer of 1991) we are entering new kinematical regions in both $Q^2 = -q^2$ and Bjorken-$x = Q^2/(2pq)$. LEP/LHC will further increase the kinematically accessible region by more than an order of magnitude. This talk will focus on the small-x region, and we shall try to answer the question to what extent LEP/LHC will see new physics in this region (for a collection of related papers see [1]).

Fig. 1 shows the connection between different high energy limits, in particular the Bjorken limit ($Q^2 \to \infty, x_{\rm Bjorken}$ fixed) and the Regge limit ($s \to \infty, Q^2 \approx Q_0^2$ fixed). The small-x region above the Bjorken limit is not far from the Regge limit: it is the continuation of the Regge limit towards large Q^2, and one therefore expects ultimately to face the same dynamics as in the Regge limit. For the discussion of the small-x limit of DIS scattering it is useful to use the variables

[1] To be published in the Proceedings of the ECFA Workshop on LHC, Aachen, FRG (1990).

[2] Supported by Bundesministerium für Forschung und Technologie, 05 4HH 92P/3, Bonn, FRG.

($\beta_0 = (11N_C - 2n_f)/3$):

$$\xi = \ln\ln\frac{Q^2}{\Lambda^2},\ y = \frac{8N_c}{\beta_0}\ln\frac{1}{x}. \tag{1.1}$$

The theoretical situation of these high energy limits can be summarized as follows. The Bjorken limit (in the horizontal direction of Fig. 1) is dominated by the light cone behavior of operator products and can therefore reliably be described by perturbation theory [2]. In particular, the renormalization group equation predicts [3,4,5] the Q^2 dependence of the moments of the structure functions. The Regge limit (in the vertical direction of Fig. 1 at low Q_0^2), on the other hand, has a strong nonperturbative component: for small momentum transfer scattering of hadrons is dominated by large transverse distances (impact parameter) and, hence, sensitive to the behavior of QCD at large distances. For the moment, no final solution to the behavior of QCD in this limit is at hand, although important work has been done [6,7,8,9,10,11,12]. In between these two regions lies the small-x limit of deep inelastic scattering (marked by the shaded area in Fig. 1): it probes the transition from the perturbative Bjorken limit to the nonperturbative region which extends the Regge limit towards large Q^2, and it thus provides the opportunity to test theoretical ideas about the onset of nonperturbative dynamics in QCD, the change from the language of quarks and gluons to that of composite hadrons. The theoretical issue to be discussed in this talk is the question how much and what we know about this transition region.

Let us first recapitulate what goes wrong with the standard QCD evolution program when x is taken to be very small. The small-x behaviour of F_2 is dominated by gluon production, and it is of the form:

$$F(x,Q^2) \approx \frac{exp\left(\sqrt{2(\xi-\xi_0)y}\right)}{\sqrt{2\pi\sqrt{2(\xi-\xi_0)}}}. \tag{1.2}$$

From this it follows that the total cross section for the scattering of a virtual photon off the proton would rise faster than any power of $\ln\frac{1}{x} \approx \ln\frac{s}{Q^2}$. Unitarity, on the other hand, requires that the growth cannot be faster than the square of the hadron radius:

$$\sigma_{tot}^{\gamma^*} = \frac{4\pi^2\alpha}{Q^2}F(x,Q^2) \le 2\pi R(s)^2,\ R(s) \approx const\cdot\ln s. \tag{1.3}$$

Somewhere in the small-x region, therefore, the standard QCD description has to become invalid.

That something new has to come in at small values of x can be seen rather easily within the parton picture [13]. The standard QCD-evolution framework can be viewed as a cascade of partonic decay processes inside the nucleon: the photon picks a quark with momentum fraction x and virtuality Q^2 (which is approximately equal to the transverse momentum squared or the inverse square of the transverse radius). Such a quark represents the final result of a chain of subsequent decay processes, in course of which the partons become slower and, at the same time, gain a larger virtuality. This picture is nothing but a space-time interpretation of the QCD-ladder diagrams shown in Fig. 2a. In the transverse (impact parameter)

plane the same situation is illustrated in Fig. 3: partons at the lower end of the ladder have still a rather low momentum scale and hence appear as "fat" in Fig. 3a. Partons at the upper end have larger virtuality and are much "thinner" (Fig. 3b and c). The number (or density) of the partons is determined by the structure functions: according to eq.(1.2) which represents the "standard QCD evolution", the number of small-x partons increases very fast. Hence, in the transverse plane their density becomes high and it becomes more and more probable that they will interact among each other. In the standard QCD framework only one type of interaction has been taken into account, namely decay processes which cause the parton density to increase. It therefore appears to be extremely suggestive to expect also other interaction processes, e.g. recombination or annihilation processes which might balance the number of partons or even decrease their density. A simple argument (Fig. 4) may illustrate how such partonic annihilation processes will modify the QCD evolution equations. In the standard scenario (Fig. 4a) a change of parton densities is obtained by a splitting of the incoming parton into two outgoing partons. Such a change δF is proportional to the probability of finding the initial parton, i.e. we have a linear evolution equation. Recombination processes (Fig. 4b), on the other hand, must be proportional to the probability of finding two incoming partons. Most naively, this probability could be assumed to be proportional to the square of the probability of having one parton: one then obtains the nonlinear term indicated in Fig. 4b. The strenght of this nonlinear term also depends upon the descent of the two incoming partons: if they originate from one common "parent" parton (e.g. one valence quark), it seems more likely that they have a chance to recombine again than for the case where they come from different valence quarks which are spatially seperated. In the first case, the strenght would be proportional to the inverse square of the quark radius, in the latter to that of the hadron.

A possible result of these creation and annihilation processes could be a "saturation" as shown in Fig. 5: the "true" QCD structure function no longer increases at small x, it approaches a constant value (up to powers of $\ln \frac{1}{x}$). Such a behaviour would also match the observed slow increase of the hadronic total cross section at low Q_0^2 in the Regge limit. Strong-field calculations within QED and QCD [14] indeed point into this direction.

This very qualitative description of small-x physics allows, in fact, a first estimate of the boundary between perturbative and nonperturbative physics in the ξ, y plane (Fig. 1). Consider the quantity

$$W(x,Q^2) = \frac{\alpha_s(Q^2)}{Q^2}\frac{F(x,Q^2)}{R^2} \approx \frac{const}{Q^2 \ln Q^2}\frac{\exp\sqrt{2\xi y}}{y^2} \qquad (1.4)$$

which measures the probability of partons to interact with each other. In order that the standard QCD casacde picture works, this probability should be less than one: neglecting all nonleading terms, this condition can be approximated by

$$y \leq const \cdot \exp 2\xi \qquad (1.5)$$

which is a very crude approximation to the upper boarder line of the transition region in Fig. 1.

In order to make these ideas more quantitative, one has to analyse sets of QCD Feynman diagrams. According to Gribov, Levin, and Ryskin [13] and Mueller and

Qiu [15] who have done such an investigation ten years ago, the first corrections to the standard QCD ladder diagrams (Fig. 2a) are diagrams of the type shown in Fig. 2b (so-called fan diagrams). The upper ladder branches into two ladders which at the lower end couple to the nucleon (in our picture only one quark line is shown; other possibilities include the coupling to two different quarks). The branching vertex (triple-ladder vertex) consists of the sum of several (nonplanar) diagrams, only one of which is shown. Taking the energy discontinuity of this set of diagrams in all possible ways, one obtains, among other contributions, the recombination process shown in Fig. 4b. However, since this set of diagrams allows for other energy cuts, the recombination process in Fig. 4 must necessarily be accompanied by other contributions. A careful analysis of all these terms leads to the well-known Abramowski-Gribov-Kancheli rules (AGK-rules) [16]. In particular, the sum of all terms carries a minus sign, relative to the ladder diagrams which correspond to the standard evolution equations. Clearly, this minus sign is highly desirable to fight the strong increase of the structure function at small x.

In the approximation where only leading powers in both lnQ^2 and $ln\frac{1}{x}$ are kept (DLA approximation), the behavior of Fig. 2 is rather simple. If we denote by $F_0(y,\xi)$ the expression for the left part of Fig. 2, then the first correction is given by:

$$-const \int^y dy_1 \int^\xi d\xi_1 F_0(y-y_1, \xi-\xi_1) V(\xi_1) F_0^2(y_1,\xi_1) \qquad (1.6)$$

where

$$V(\xi) = \frac{3\pi^2}{4\beta_0}\frac{Q_0^2}{\Lambda^2}\exp\{-e^\xi - \xi\} \equiv C\,\exp\{-e^\xi - \xi\} \qquad (1.7)$$

stands for the triple ladder vertex.

In order to proceed further, Gribov, Levin, and Ryskin made an assumption concerning the coupling of $n \geq 2$ ladders to the hadron: this coupling is assumed to be proportional to the n-th power of the single-ladder coupling. As a consequence, the probability of finding two gluons (at low momentum Q_0^2) with momentum fractions x_1 and x_2 is proportional to $g(x_1,Q_0^2)\cdot g(x_2,Q_0^2)$. This assumption then allows to find an equation for the sum of all fan diagrams, the GLR equation. It is a nonlinear integro-differential equation. In its simplest form, the DLA approximation, it is obtained by generalizing eq.(1.6) and performing the sum over all ladders:

$$F(y,\xi) = F_G(y,\xi) - \int_0^y dy' \int_{\xi_0}^\xi d\xi' F_0(y-y', \xi-\xi') C \exp\left(-e^{\xi'} - \xi'\right) F^2(y',\xi'). \qquad (1.8)$$

where C stands for the constant factors of (1.7), and F_G denotes the sum of QCD ladder diagrams with some initial distribution $G(y)$. The more accurate form of the equation is given as:

$$\frac{\partial\phi(x,q^2)}{\partial \ln(\frac{1}{x})} = \int \tilde{K}(q^2,q'^2)\phi(x,q'^2)\frac{4N\alpha_s(q'^2)}{4\pi}dq'^2 - \frac{1}{4\pi R^2}\left(\frac{\alpha_s(q^2)}{4\pi}\right)^2 V\phi^2(x,q^2). \qquad (1.9)$$

Here $\phi = \frac{\partial F}{\partial Q^2}$, R denotes the transverse radius of the hadron (or quark), and V stands for the triple ladder vertex, evaluated more accurately than in (1.7), namely in the semiclassical approximation.

Among the few features that are known [13,17] about analytic solutions to these nonlinear equations, we only mention one, namely the existence of a well-defined line in the x, Q^2 plane which marks the beginning of the nonperturbative regime. It is approximately of the form

$$y = \frac{1}{4}\left(\ln\frac{Q^2}{\Lambda^2}\right)^2 + const, \tag{1.10}$$

and in Fig. 1 it is the upper boarder line of the transition region. The exact position of this "critical" line depends upon the initial conditions and can be determined only numerically. Above this line, the GLR equation is no longer valid, and the dynamics is excpected to be very similar to that of the Regge limit.

2 Numerical Estimates

In the context of LEP/LHC (and also HERA) one of the most important question seems to be: where in the (x, Q^2)-plane lies the transition region, i.e. that region for which the GLR equation should replace the standard QCD evolution scheme? To answer this one has to solve the GLR-equations numerically. So far there exist two calculations [17,19]. They both solve the the DLA approximation (1.8), but inside the QCD gluon ladders they use the full Altarelli-Parisi splitting functions for the rungs.

As we have explained before, the numerical solution depends upon two input quantities, the initial y-distribution at some low Q_0^2 and the strenght C of the nonlinearity. [17] therefore uses two different input distributions, and both papers vary the parameter C by a factor of 10 or 2.5, respectively. Predictions for the (momentum weighted) gluon distribution are shown in Figs. 7 and 8, for F_2 in Fig. 9. In Fig. 7, the full curves correspond to the nonlinear evolution: the upper ones to the (steeper) Morfin-Tung initial [20] distribution, the lower ones to the (almost flat) Eichten-Hinchclife-Lane-Quigg [21] distribution. The dashed and the dotted curves show the corresponding results of the standard (linear) evolution programs for two different values of C: the lower curves belong to the larger value eq. (1.7), for the upper ones C is divided by ten. The main point to be emphasized is the fact that e.g. for $Q^2 = 10GeV^2$, deviations are visible already at x close to 10^{-2}. For the larger of the two C-values this effect is, of course, more pronounced than for the smaller one. Fig. 6 shows an approximate estimate of the transition region. The critical curve which marks the boundary between the perturbative and the nonperturbative domains can be written as

$$Q_c^2(x) = Q_0^2 + \Lambda^2 \exp\left(c_1\sqrt{\ln\frac{x_0}{x}}\right). \tag{2.11}$$

Levin and Ryskin [22] estimated $\Lambda = 52\,\mathrm{MeV}$, $Q_0^2 = 2\,\mathrm{GeV}^2$, $c_1 = 3.56$, and $x_0 = 1/3$, whereas in [17] the parameters are $\Lambda = 212\,\mathrm{MeV}$, $Q_0^2 = 0$, $c_1 = 3.39$, and $x_0 = 1/15.9$. The two estimates are shown as curves 1 and 2 in Fig. 6, respectively. The region of validity of the standard evolution is estimated to lie below the tangent in the (y, ξ)-plane to the boundary line at $\xi = \xi_0$. This line is shown as curve 3 in Fig. 6.

Figs. 8 and 9 show results of [19] for $xg(x, Q^2)$ and $F_2(x, Q^2)$, respectively. In this case the input distribution is again a rather steeply rising function in y; its analytic form has been motivated by the analysis of [24]. Deviations between the linear and the nonlinear evolution start at x between 10^{-2} and 10^{-3}, quite in agreement with the findings of [17]. [19] also presents results for F_2: it is, however, not clear whether this calculation takes into account certain difficulties which have been pointed out in [25]: once the gluon structure function has been calculated from the GLR-equation, the quark loop which couples the gluons to the deep inelastic photon, can no longer be used in the leading-Q^2 approximation.

The important message of these two papers seems to be that, provided the x-distribution at low Q^2 is as steeply rising as it was assumed in most of these calculations, already HERA will enter the region where the "new" physics is at work (to be more precise, since at these relatively small values of $Q^2 \approx 10GeV^2$ the "intermediate" region between perturbative and nonperturbative QCD is very narrow, HERA not only enters this transition region but also reaches into the domain of nonperturbative QCD). However, this does not necessarily imply that it will be possible to conclude from HERA measurements of structure functions beyond any doubt, whether one sees this new physics or not. Due to our ignorance of the correct x-distribution at low Q_0^2 which always enters the calculation as an input, it is possible that the measurement of some flat structure function can be descibed very well by the standard evolution, using some modified input function. Conversely, a continuing rise of the structure function at low x is not necessarily a reliable indication that the "new physics" is not yet at work. The best way to distinguish is the comparison of evolution in Q^2: linear and nonlinear evolution equations predict different Q^2-dependence. In order to extract this from data we need a range in Q^2 as large as possible: this is the point where LEP/LHC will be most powerful. By offering, at, say, $x = 10^{-4}$, a substantially larger range in Q^2 than HERA, it will be possible to distinguish much better between "standard" and "new" physics than at HERA.

It will still be desirable to look for experiments which are specially designed to probe the "new physics". So far, two such measurements have been proposed. The one is due to A.Mueller [14] and refers to the "hot spots" , the other one uses the diffractive dissociation of the photon and has been proposed by Ryskin [22]. Returning to the discussion on "saturation" in Part I of this talk, the density of gluons in the transverse plane may not be uniform, i.e. there may be regions inside the nucleon (Fig. 3) which are more densely populated by soft gluons than others. Since the structure function F_2 ("total photon hadron cross section") measures the parton density, averaged over the full size of the hadron, one needs to look at exclusive final states which measure the distribution of partons inside limited subregions of the hadron (Fig. 3b). Such an experiment is illustrated in Fig. 10: measure the cross section of jets which carry the momentum fraction x (not to be confused with the usual Bjorken x_B which belongs to the photon at the upper end) and the momentum scale (transverse momentum squared) $k_\perp^2$. The latter should be not much smaller than Q^2, the mass of the photon: $R_{parton}^2 \approx \frac{1}{Q^2}$ is the transverse radius of the parton struck by the photon, and $R_{jet}^2 \approx \frac{1}{k_\perp^2}$ is the square of the average transverse distance, by which the jet is seperated from this parton. If $k_\perp^2 \leq Q^2 \ll Q_0^2$, then $R_{parton}^2 \leq R_{jet}^2 \ll R_{hadron}^2$, and this process explores the

parton cloud of diameter R_{jet} around the struck parton. The cross section should be measured as a function of the ratio $\frac{x_B}{x}$, and the region of interest is defined as $x_B \ll x$. The cross section for this process is, in the QCD-parton model, given by:

$$\frac{k_\perp^2 x d(\nu W_2}{dx dk_\perp^2} = C\alpha(Q^2)\left(xg(x,k_\perp^2) + \frac{4}{9}(xq(x,k_\perp^2) + x\bar{q}(x,k_\perp^2))\right) F(\frac{x_B}{x}, Q^2, k_\perp^2) \tag{2.12}$$

where C is a normalization factor, $q(x,q^2)$ and $g(x,q^2)$ are the quark and gluon distribution functions, resp., and $F(\frac{x_B}{x}, Q^2, k_\perp^2)$ stands for the sum of QCD ladders above the jet, evaluated in the limit $\frac{x_B}{x} \to 0$ (this is one of the places where the so-called "Lipatov Pomeron" [10] could be tested). This formula predicts a steep rise as $\frac{x_B}{x}$ becomes small:

$$F(\frac{x_B}{x}, Q^2, k_\perp^2) \approx C \frac{\exp\left(\frac{12\alpha(Q^2)}{\pi} \ln 2 \ln \frac{x}{x_B}\right)}{\sqrt{\ln \frac{x}{x_B}}} \tag{2.13}$$

and a deviation from this would be indicative of "local saturation", i.e. the existence of a "hot spot". Corrections to this formula can (and should) be calculated: these are not fan-diagrams but reggeon diagrams, since both Q^2 and $k_\perp^2$ are of the same order.

Another strong prediction based upon the existence of such "hot spots" has been made by Ryskin [26]. Instead of the "one-jet inclusive cross section" of Fig. 10 one considers the photon diffractive dissociation processes shown in Fig. 11 (its connection with the Pomeron structure function [28,29,30] has been discussed in [27]): there is a rapidity gap between the proton at the lower end and the missing mass cluster above. As an example, this missing mass final state could consist of three jets, originating from $q\bar{q}g$. The final states are further restricted by the requirement that the jet in the direction of the Pomeron should have a controllable $k_\perp$. It is then the dependence upon this $k_\perp$ which differentiates between "saturation" and "standard" QCD behavior: with saturation the cross section should be substantially smaller, and for the integrated cross section there could be a difference up to a factor of one hundred!.

There are clearly more measurements that might be suitable to test the presence of the "new physics" described in the this talk: this will not be discussed here and should be a topic of further theoretical work.

3 Measurements at small-x

In this section we report about the prospects to actually measure structure functions and parton distribution functions at LEP+LHC in the small-x region. We will discuss measurements of F_2 as well as various ways to extract the gluon densities. All analyses performed so far use the conventional approach in the evolution of the parton densities. This is certainly sufficient to estimate the limits on the explorable regions in x and Q^2 for a given reaction. Our compilation of the various kinematic ranges allows an overview of the overlaps and the gaps in the determination of parton distributions. Furthermore, first estimates on prospects to observe new physics can be drawn, e.g. one can find how much of the evolution in Q^2 may be seen at a given values of x. Clearly, new calculations of cross sections and

differential distributions based on the improved evolution scenario are necessary to eventually set limits on the quantities parametetrizing the new effects.

We start by discussing the structure function F_2 which is obtained in inclusive lepton scattering from a measurement of the differential cross section $d^2\sigma/dxdQ^2$. Assuming the validity of the standard evolution one predicts large rates for (neutral current) deep inelastic ep scattering in the small-x region at LEP/LHC[31]. At small-x the kinematical variables x and Q^2 and thereby $d^2\sigma/dxdQ^2$ can well be reconstructed via a measurement of the scattered electron. The kinematic region accessible to (possible) experiments is investigated in detail in ref.[32]. Here we show in Fig. 12 (label F_2) the region which is accessible in inclusive DIS via measurements of the scattered electron, if LEP/LHC is run with 50 GeV electrons on 8000 GeV protons. Changes of the beam energies will shift the accessible region accordingly[32]. As one can see from Fig. 12, LEP/LHC at $\sqrt{s} = 1.26\,\mathrm{TeV}$ allows measurements down to $x \approx 6 \times 10^{-6}$ at still high Q^2 ($Q^2 > 10\,\mathrm{GeV}^2$). At a given value of x about one order of magnitude in Q^2 can be covered. This range is extended if LEP/LHC is run at lower and higher cms energies. From the relation $Q^2 = xys$ with $y < 1$ it becomes clear that small-x values imply also small values for Q^2. Thus for $x < 10^{-3}$ weak effects can be neglected[31] and the measurements at small-x are then sensitive to the electromagnetic structure function $F_2^{em} = \sum_f e_f^2[q_f(x,Q^2) + \bar{q}_f(x,Q^2)]$. Thus it is the total quark sea which is being probed. The prospects of unfolding individual components of the (sea) quark distributions are studied in [31].

An ep collider offers several ways to measure the gluon density. Inclusive electron scattering is sensitive to the gluon either via the Q^2 evolution of a (singlet) structure function or via the longitudinal structure function $F_L(x,Q^2)$. Among the exclusive processes heavy quark production appears most promising to extract the gluon density. The interest in the gluon distribution arises not only from its increasingly importance for predicting cross sections and distributions at hadron colliders at higher energies. As mentioned above, screening corrections are expected to set in earlier in x for the gluon density than for the quark densities. Moreover, it is the gluon which "drives" the evolution equations at small-x.

There are several problems in the determination of the gluon density from the Q^2 evolution of F_2: (i) the restricted Q^2-range at fixed-x (c.f. Fig. 12); (ii) the unknown value of Λ_{QCD} which has to be fitted together with the gluon density (see e.g. [33]); and (iii) the validity of the evolution equations. It is well known that DIS data alone do not allow to fix the parameters of the gluon distribution very precisely (even if the standard evolution is assumed to be valid), and Drell-Yan data (and possibly direct-photon data) are usually added to obtain more severe constraints (see e.g. [34]). If screening corrections are taken into account then the use of an improved evolution equation requires the fit of at least one more parameter (e.g. the quantity C in eq. 1.7). Further development of computer algorithms for the nonlinear evolution equations is needed before reliable estimates on gluon determination from this method can be made. Extrapolating present day limits [34] we can crudely estimate a range

$$0.0005 < x < 0.03 \quad , \quad Q_0^2 \approx 5\,\mathrm{GeV}^2 \tag{3.14}$$

in which the gluon distribution $G(x,Q_0^2)$ at an input scale Q_0^2 might be determined. This range is shown as dashed line labeled $\partial F_2/\partial \ln Q^2$ in Fig. 12.

Another way of determing the gluon density makes use of data in the $25 \lesssim Q^2 \lesssim 150\,\mathrm{GeV}^2$ region[33]. At small-x, the ratio $R = \sigma_L/\sigma_T$ in DIS is expected to be relatively large due to the contribution to the longitudinal structure function F_L from the glue: the gluon initiated contribution I_G dominates over the quark contribution I_F in $F_L(x,Q^2) = 4\alpha_s(Q^2)/(3\pi)\,[I_F + 5/3\,I_G]$. In fact, at small-$x$, the value of F_L is essentially proportional to the gluon distribution at a re-scaled value of x[35]. An accurate measurement of F_L in this region is thus a direct probe of the gluon distribution. Experimentally, F_L can be disentangled from the differential cross section at *fixed* x and Q^2 by combining measurements at various cm energies. Thus this method yields the gluon density $G(x,Q^2)$ differential in x and Q^2. The corresponding study for LEP/LHC was performed in [36]. The explorable kinematic range was estimated to

$$\begin{aligned} 6.3\times10^{-5} < x < 2.5\times10^{-4} \quad &\text{at} \quad Q^2 = 25\,\mathrm{GeV}^2 \\ 3.8\times10^{-4} < x < 1.5\times10^{-3} \quad &\text{at} \quad Q^2 = 150\,\mathrm{GeV}^2 \end{aligned} \tag{3.15}$$

and is shown in dash-dots labeled F_L in Fig. 12. Within this region different gluon parametrizations should clearly be distinguishable. This is illustrated in Fig. 13 which shows two different gluon distributions superimosed on measurements expected at LEP/LHC. The error bars include both statistical and sytematic errors. To arrive at the region (3.15), it was assumed in [36] that LEP/LHC is run at four different machine set ups, ranging from $E_p \times E_e = 2000\times40\,\mathrm{GeV}^2$ to $8000\times50\,\mathrm{GeV}^2$ with an integrated luminosity of $100\,\mathrm{pb}^{-1}$ each.

Parton densities can also be measured in exclusive final states. Here one faces two problems. First, in contrast to lepton inclusive scattering, the (momentum) scale argument μ of the parton densities is not uniquely defined. In quasi-real photoproduction, for example, Q^2 is much smaller than $1\,\mathrm{GeV}^2$. The scale μ that governs high p_T reactions is then $\hat{s}$ or p_T^2 rather than Q^2. Second x_p, the momentum fraction of the struck parton is no longer equal to Bjorken-x, $x_p > x$ in general. The procedure to measure a specific parton density is then the following one: First one has to isolate those events which are sensitive to the desired distribution. Then one tries to reconstruct kinematical variables which constraint x_p and μ.

Thus far only the prospects of measuring the gluon density have been considered [37]. Because of the large rates, the clean (leptonic) signatures, and the fact that the leading order production mechanism is photon-gluon fusion, the production of heavy quarks looks most promising. In [37] a systematic investigation of gluon extraction from heavy quark production in ep collisions has been performed. Here it is shown that the gluon density can succesfully be reconstructed from heavy quark production in ep collisions. The analysis is based on complete (signal and background) events and, in the case of J/Ψ, it includes a full detector simulation. The reconstruction of the event kinematics is outlined, in particular uncertainties due to unsufficient known fragmentation properties of the proton remanats and photon spectator jet are discussed. Higher order corrections on the event topology are approximately taken into account by multiple gluon radiation in a parton cascade approach. Only information obtainable from a main detector is used. In a previous study on gluon extraction from J/Ψ events at HERA[38] the information on the scattered electron coming from a luminosity monitor measurement has been used. This is not done in [37] since it is not clear whether such a device will

work with the high rates expected at LEP/LHC. Furthermore it was found that with the main detector a much larger range in x is accessible, including the range reachable via the luminosity measurement. The outcome is that one will obtain measurements of $d\sigma/dx_g$ which are accurate enough to extract the gluon density, and hence to distinguish between different parametrizations.

In general, unknown higher order corrections introduce systematical (theoretical) uncertainties. For the purpose of extracting the gluon density along the lines of [37] it is necessary to have available the full one-loop corrections of the di-heavy quark invariant mass and rapidity distributions, or even better the fully differential cross section evaluated at next-to-leading-order (NLO). Such a calculation needs in addition a correct treatment of the bound state system to that order for J/Ψ events. A consistent NLO calculation requires the inclusion of the resolved photon processes with appropriate caveats of double counting the collinear contributions. Thus the results of [37] have to be interpreted as the extraction of the leading order gluon density. A determination accurate to NLO would require the implemention of the above mentioned corrections.

With these caveats in mind let us discuss the result of the analysis in [37]. In J/Ψ production the gluon density may be determined at an average scale in a range of:

$$3\times10^{-5} < x < 1\times10^{-2} \quad \text{at} \quad Q^2 \approx 25\,\mathrm{GeV}^2 \tag{3.16}$$

This is shown as solid line in Fig. 12. The scale Q is identified with the invariant mass $\sqrt{\hat{s}}$ of the subsystem and not to be confused with the (almost zero) virtuality of the exchanged photon. For open heavy quark production the average scale of the gluon density increases with x_g. Here one finds

$$6\times10^{-5} < x < 5\times10^{-2} \quad \text{at} \quad Q^2(x_g) \approx \sqrt{x_g}\,10^4\,\mathrm{GeV}^2 \tag{3.17}$$

which is shown as dashed line in Fig. 12. The larger lower limit of x_g arises from the fact that harder cuts are necessary to trigger and identify open heavy quark events. The rates are large enough to allow a binning in the scale. Thus actually a range in both x and Q^2 (full line labeled $Q\bar{Q}$ in Fig. 12) can be probed:

$$\begin{aligned} 400 < \mu^2 < 1600\,\mathrm{GeV}^2 \quad &\text{at} \quad x_g = 0.001 \\ 2300 < \mu^2 < 7800\,\mathrm{GeV}^2 \quad &\text{at} \quad x_g = 0.020 \end{aligned} \tag{3.18}$$

opening the prospects of observing the evolution of the gluon density in open heavy quark production at LEP/LHC. The discriminative power is illustrated in Figs. 14 and 15 where two different gluon distributions superimposed on measurements expected at LEP/LHC are shown. The error bars include the statistical and (experimental) systemantic errors.

In comparing the different kinematic regions of Fig. 12 we find that the J/Ψ and F_L measurements partly overlap. The smallest value in x of the gluon density can probably be obtained through measurements of J/Ψ events. Open heavy quark production extends the x region towards higher x and scale Q values. The heavy quark results are obtained assuming that LEP/LHC is run solely at a fixed cms energy ($\sqrt{s} = 1.26\,\mathrm{TeV}$). Data at different cms energies are highly desirable also in this case. This will not only allow to check the theoretical predictions and to put the description of the events on a firmer basis. Since there is strong correlation

between the average scale and the cms energy in the case of open heavy flavour production runs of LEP/LHC at various cms energies would allow measurements of the gluon density over an extended $\{x, Q^2\}$ region, bridging the gap between the F_L and the $Q\bar{Q}$ measurements of the glue. If we finally compare the kinematic ranges of Fig. 12 with predictions for the boundary lines in fig. 6 then we find that LEP/LHC can clearly probe the transition region better than HERA (and also better than hadron colliders). Furthermore the nonperturbative regime will be entered with a comfortable range in Q^2 allowing a study of the dynamical behaviour of this new region.

4 Summary

The *ep* option LEP/LHC will enable us to explore a new domain in deep inelastic scattering, namely the region of very small Bjorken-x. Measurements will extend down to $x < 10^{-5}$ for, say, $Q^2 \geq 10\,\mathrm{GeV}^2$, i.e. for values of Q^2 where α_s is small. From the theoretical viewpoint, this kinematic region is interesting since it lies at the interface between perturbative and nonperturbative QCD: for moderate (i.e. not too small) x-values, we have the well-tested QCD evolution equations of Gribov, Lipatov, Altarelli, and Parisi, whereas in the extreme small-x limit one reaches the nonperturbative Regge limit which we do not yet fully understand. Generally one expects that the "true" structure functions at small x are smaller than the extrapolation of the standard QCD evolution equation. One attractive possibility is "saturation", i.e. a flattening of the structure function.

In between these two domains lies a transition region, where one might hope to see, still using perturbative QCD, the beginning of the transition to nonperturbative physics. For this region Gribov, Levin and Ryskin suggested a new, nonlinear evolution equation. It results from a careful analysis of large classes of Feynman diagrams (and also relies upon a certain assumption), and investigations of solutions (both analytically and numerically) have only been started. Although the validity of this equation in the x-Q^2 plane is limited and does not extend into the nonperturbative region, its predictions for this region are consistent with unitarity and, in particular, with the idea of "saturation".

Existing numerical estimates indicate that HERA and even more LEP/LHC will not only enter this transition region but also reach the nonperturbative regime. The advantage of LEP/LHC over HERA is the possibility to observe the small-x behavior over a much larger range in Q^2, i.e. to distinguish between the Q^2 evolution *à* la Alrarelli-Parisi and Gribov, Lipatov, and Ryskin.

So far effects of the nonlinear evolution have been calculated only for the inclusive distributions F_2 and the gluon structure function. So practically all existing estimates of possible measurements at small-x assume the validity of the standard (linear) evolution and have to be redone, taking into account the effects of the "new" physics. Particular attention has to be given to special measurements which are sensitive to the onset of the "new" physics. Examples are the "hot spots" or photon diffractive dissociation.

Moreover we feel it necessary to further develop new computer programs based on the improved evolution equations. Analytic studies of the GLR-equation have shown several aspects which have to be taken into account when using these equations. One is the fact that the input distributions at fixed Q_0^2 should be prescribed only for a finite x-interval. Second, it may be useful to analyse the data along particular lines in the x-Q^2 plane, the so called "classical paths". This may be the best way to distinguish between "standard" and "new" physics and also determines the boundary line between perturbative and nonperturbative physics.

As to practical measurements, at small-x the contribution of the gluon density to the cross sections becomes more and more important. Measurements of the longitudinal structure function F_L are estimated to be precise enough to extract the gluon density down to $x = 6.3 \times 10^{-5}$ (at $Q^2 = 25\,\mathrm{GeV}^2$). Additional information on the gluon distribution in a somewhat different part of the small-x region can be obtained from heavy quark production.

Let us finally emphasise the importance of running LEP/LHC at various cms energies. First, this will enlarge the Q^2 range accessible to F_2 measurements at fixed x. This clearly increases the resolution power for new physics. A larger lever arm in Q^2 also increases the sensitivity to the glue as well as allows a better determination of Λ. Second, several cms energies are necessary to extract the gluon density via measurements of F_L, theoretically the most appealing method. Last not least the range accessible to gluon measurements in heavy quark production is extended. Even more important, this allows for tests of the production mechanims of heavy quark quarks and thus to control the theoretical systematic errors.

References

[1] *Proceedings of the Small-x Workshop*, held at DESY, May 1990 (to be published in *Nucl.Physics*, ed.A.Ali and J.Bartels).

[2] For general reviews on perturbative QCD see, e.g.:
H.D.Politzer, *Phys.Rep.* **14C**, 129(1974);
C.H. Llewellyn Smith, Schladming Lectures 1987, *Acta Phys. Austr. Suppl. XIX*, 331(1978);
Yu. Dokshitzer, D.I. Dyakonov, S.I. Troyan, *Phys.Rep.* **58**, 269(1980);
E.Reya, *Phys.Rep.* **69**, 195(1981); A.H.Mueller, *Phys.Rep.* **73**, 237(1981);
G.Altarelli, *Phys.Rep.* **81**,1 (1982).

[3] V.N. Gribov and L.N. Lipatov, *Sov. Journ. Nucl. Phys.* **15**, 438 and 675 (1972).

[4] G.Altarelli and G.Parisi, *Nucl.Phys.* **126**, 297(1977).

[5] Yu.L..Dokshitser, *Sov.Phys.JETP* **46**, 641(1977).

[6] E.A.Kuraev, L.N.Lipatov, V.S.Fadin, *Sov.Phys.JETP* **44**, 443(1976).

[7] E.A.Kuraev, L.N.Lipatov, V.S.Fadin, *Sov.Phys.JETP* **45**, 199(1977).

[8] Ya.Ya.Balitzky, L.N.Lipatov *Sov.Jour.Nucl.Phys.* **28**, 822(1978).

[9] Ya.Ya.Balitzky, L.N.Lipatov *JETP Letters* **30**, 355(1979).

[10] L.N.Lipatov, *Sov.Phys.JETP* **63**, 904(1986) and references therein.

[11] J.Bartels. *Nucl.Phys.* **B151**, 293(1979); *Nucl.Phys.* **175**, 365(1980); *Acta Phys.Pol.* **B11**, 281(1980); unpublished.

[12] A.R.White, ANL-HEP-PR-90-28 and references therein.:

[13] L.V.Gribov, E.M.Levin, and M.G.Ryskin. *Phys. Rep.* **100**, 1 (1982)

[14] A.H.Mueller, *Nucl.Phys.* **B307**, 34 (1988); *Nucl.Phys.* **B317**, 573(1989); *preprint Columbia Univ.* **CU-TP-441**.

[15] A.H.Mueller and J.Qiu, *Nucl.Phys.* **B268**, 427 (1986).

[16] V.A. Abramovsky, V.N. Gribov, O.V. Kancheli, *Sov. Journ. Nucl. Phys.* **18**, 595(1973).

[17] J. Bartels, J. Blümlein and G.A. Schuler, DESY 90-91 and to appear in Zeitschrift für Physik C.

[18] A.H.Mueller, to appear in the *Proceedings of the Small-x Workshop*, held at DESY, May 1990 (to be published in *Nucl.Physics*, ed.A.Ali and J.Bartels);

[19] J. Kwiecinski, A.D. Martin, W.J. Stirling, and R.G. Roberts, Rutherford Preprint RAL-90-053

[20] J.Morfin and Wu-Ki Tung, preprint Fermilab-Pub 90/74 (1990).

[21] E. Eichten et al., Rev. Mod. Phys. **56** (1984) 579 and Erratum **58** (1986) 1065.

[22] M.G.Ryskin. *Sov.Journ.Nucl.Physics* **47**, 230 (1988).

[23] J.Collins and J.Kwiecinski, *Nucl.Phys.* **B316**, 307 (1988).

[24] J.Collins and J.Kwiecinski, *Nucl.Phys.* **B335**, 89 (1990).

[25] E.M.Levin and M.G.Ryskin, Frascati Preprint April 1990.

[26] M.G.Ryskin. DESY 90-050 and to appear [1].

[27] J.Bartels, G.Ingelman, *Phys.Lett.* **235B**, 175 (1990).

[28] G.Ingelman and P.Schlein, *Phys.Lett.* **152B**, 256(1985).

[29] H.Fritzsch and H.H.Streng, *Phys.Lett.* **154B**, 391(1985).

[30] E.L.Berger, J.C.Collins, D.E.Soper, G.Sterman, *Nucl.Physics* **B286**, 704 (1987).

[31] G. Ingelman, *LEP/LHC deep inelastic scattering: structure functions and final states*, to be published in the Proceedings of the ECFA Workshop on LHC, Aachen, FRG (1990).

[32] J. Feltesse, *Experimentation at LEP/LHC*, to be published in the Proceedings of the ECFA Workshop on LHC, Aachen, FRG (1990).
J. Blümlein, J. Feltesse and M. Klein, *Kinematics and reconstruction at LEP/LHC*, to be published in the Proceedings of the ECFA Workshop on LHC, Aachen, FRG (1990).

[33] A.D. Martin, R.G. Roberts and W.J. Stirling, Phys. Rev. **D37** (1988) 1161.

[34] J.G. Morfin, Fermilab-Conf-90/155, and in Proceedings of the workshop on hadron structure functions and parton distributions, Batavia, Illinois, April 1990.

[35] A.M. Cooper-Sarkar et al., Z. Phys. **C39** (1988) 281, and in Proceedings of the HERA workshop, DESY, Hamburg 1987.

[36] N. Magnussen and G.A. Schuler, *Extracting the gluon density from the longitudinal structure function F_L*, to be published in the Proceedings of the ECFA Workshop on LHC, Aachen, FRG (1990).

[37] K.J. Abraham, H. Jung, G.A. Schuler and J.F. de Trocóniz, *Gluon extraction from charm and bottom production at LEP/LHC*, to be published in the Proceedings of the ECFA Workshop on LHC, Aachen, FRG (1990).

[38] S.M. Tkaczyk, W.J. Stirling and D.H. Saxon, in Proceedings of the HERA workshop, DESY, Hamburg 1987.

Figure Captions

Fig. 1: Different High Energy Limits.

Fig. 2: QCD ladders (a) and the first correction (fan diagram, b).

Fig. 3: Partons in the transverse plane (impact parameter plane).

Fig. 4: Partonic subprocesses: (a) splitting of partons, (b) partonic recombination process.

Fig. 5: Small-x behavior of the structure function: standard QCD evolution versus"true QCD" evolution. Labels A, B, and C denote the region of perturbative QCD, the transition region and the nonperturbative region, respectively.

Fig. 6: The transition region in the (x, Q^2) plane. The lines are defined in the text, eq. (2.11) and below.

Fig. 7: x-distributions of $xg(x, Q^2)$ for the model of [17] for different values of Q^2. The full lines always belong to the linear equation ($C = 0$), the dashed ones to the nonlinear case with C of eq.(2.3), and the dotted ones to the nonlinear case with $\frac{1}{10}C$.

Fig. 8: x-distributions of $xg(x, Q^2)$ for different values of Q^2 (from [19]): the solid line belongs to the linear evolution. The dashed and the dot-dashed lines are the results of the nonlinear evolution; in the second case the nonlinearity parameter is increased by a factor of 2.5, compared to the first one.

Fig. 9. x-distributions for $F_2(x, Q^2)$ (from [19]): for the upper three curves the notation is the same as for Fig.8. The dotted curve corresponds to another input distribution (which is flat for $x \to 0$).

Fig. 10: A final state configuration which probes the "Hot spot".

Fig. 11: Final state configuration for photon diffractive dissociation.

Fig. 12: Kinematic region in x and Q^2 explorable at LEP/LHC.

Fig. 13: Measurement of the gluon distribution from the longitudinal structure function F_L [36]. Two different gluon distributions are superimposed on the measurments expected for data at LEP/LHC. The error bars indicate the size of the (combined) statistical and systematic errors.

Fig. 14: Measurement of the gluon distribution from inelastic J/Ψ production[37]. Two different gluon distributions are superimposed on the measurments expected for data at LEP/LHC. The error bars indicate the size of the (combined) statistical and (experimental) systematic errors.

Fig. 15: Measurement of the gluon distribution from open heavy quark production[37]. Two different gluon distributions are superimposed on the measurments expected for data at LEP/LHC. The error bars indicate the size of the (combined) statistical and (experimental) systematic errors.

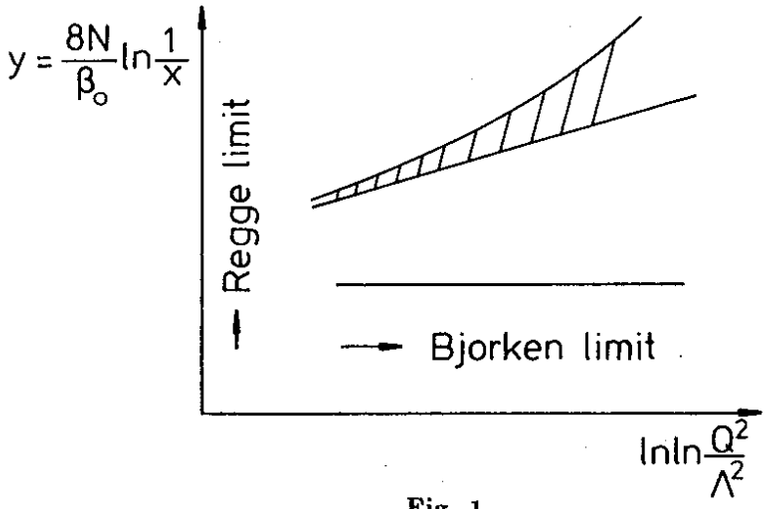

Fig. 1

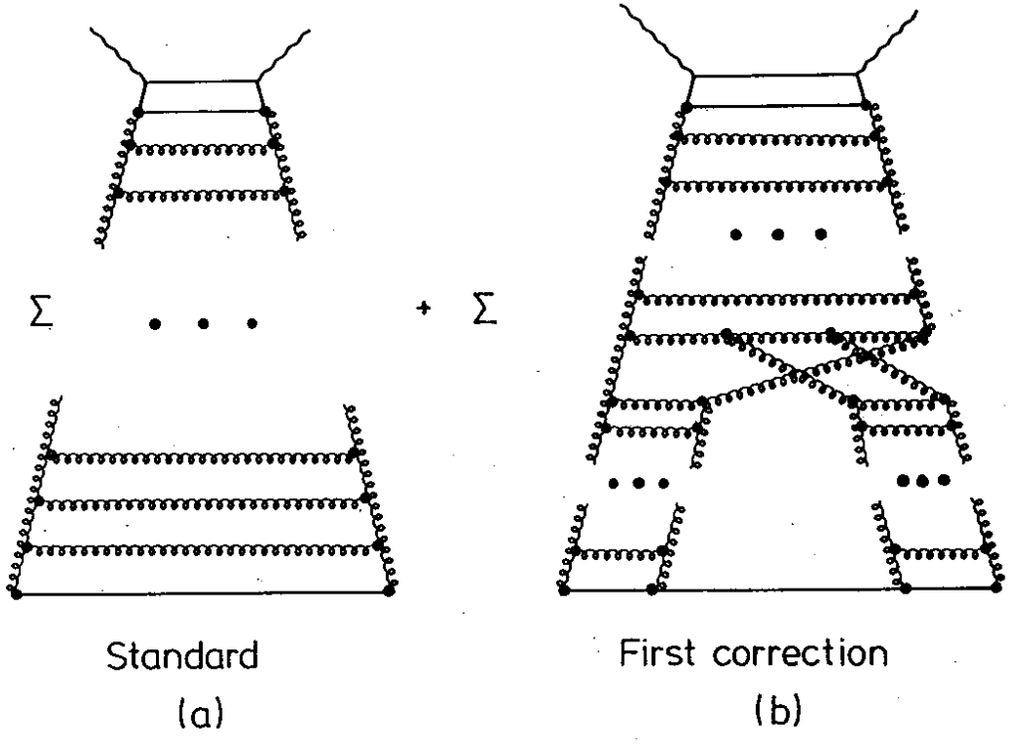

Fig. 2

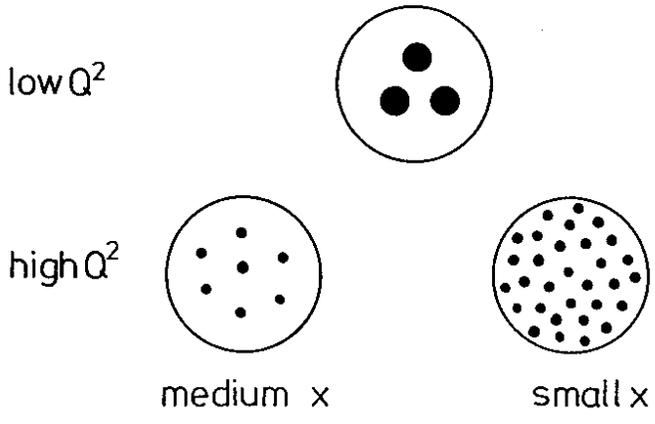

Fig. 3

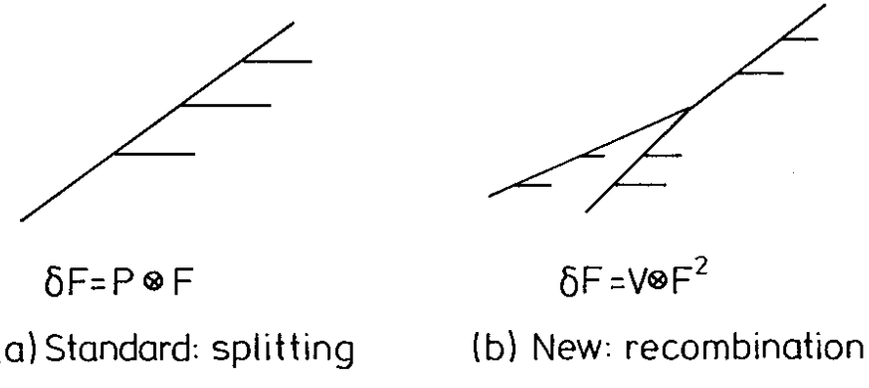

Fig. 4

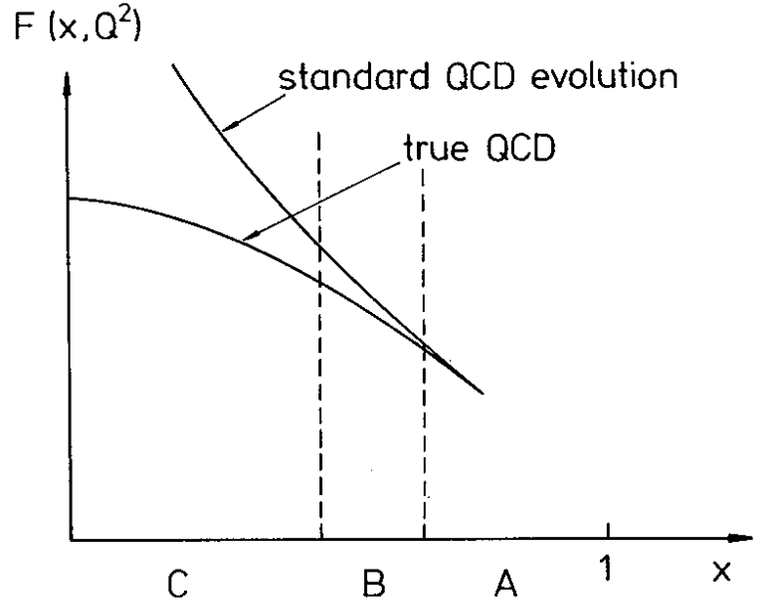

Fig. 5

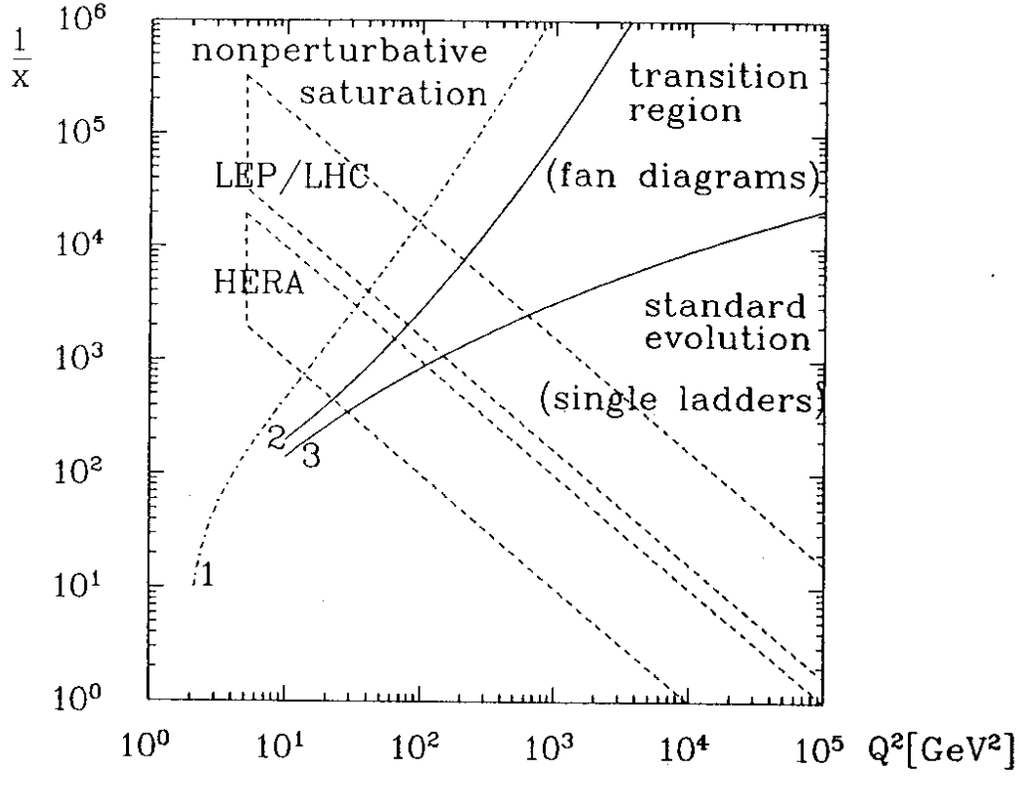

Fig. 6

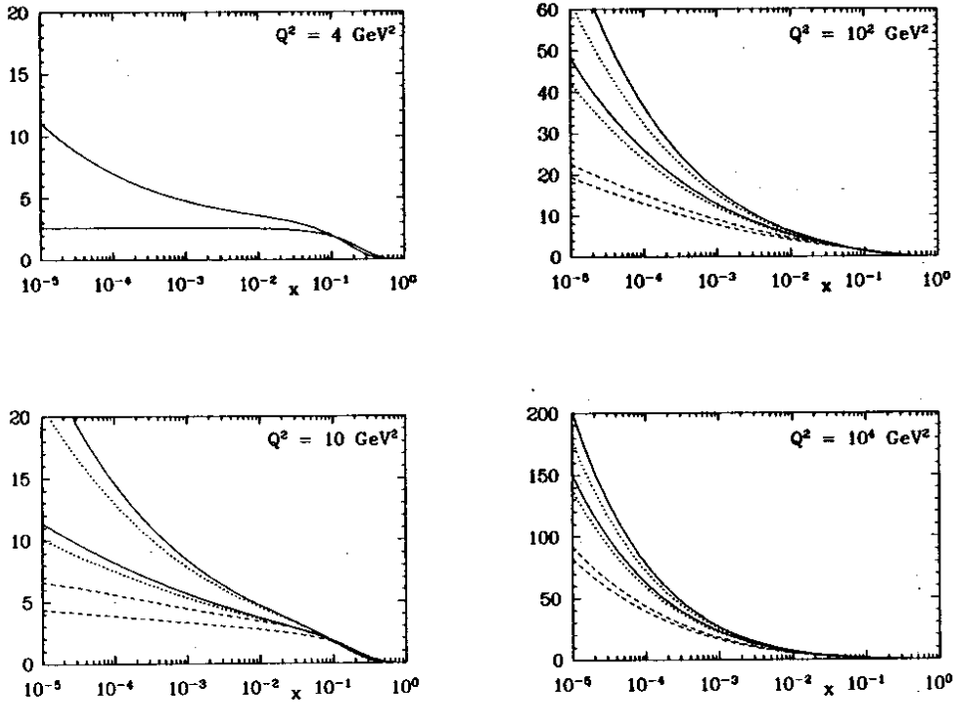

Fig. 7

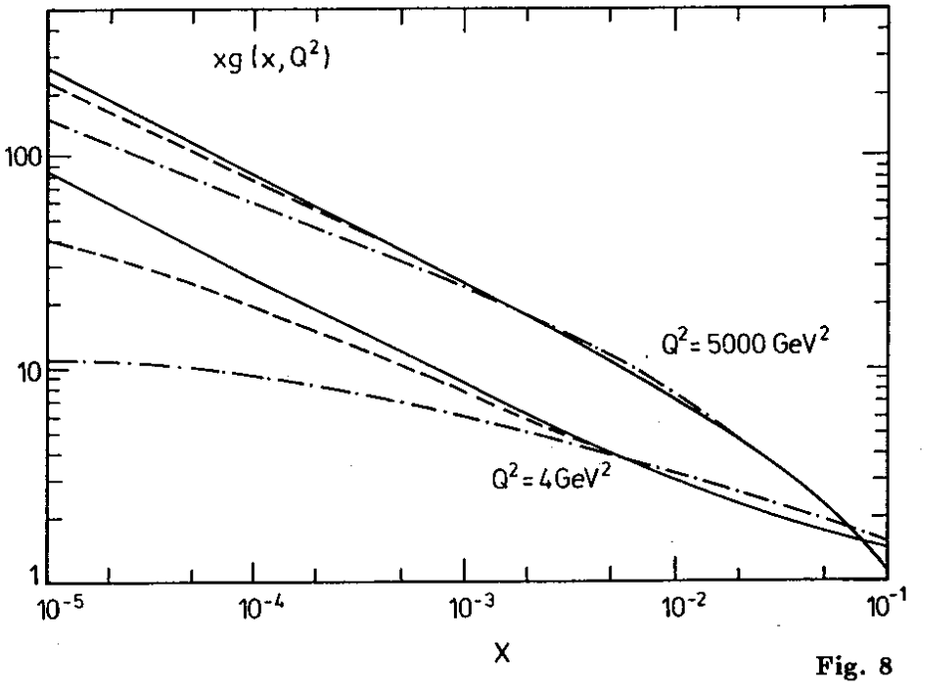

Fig. 8

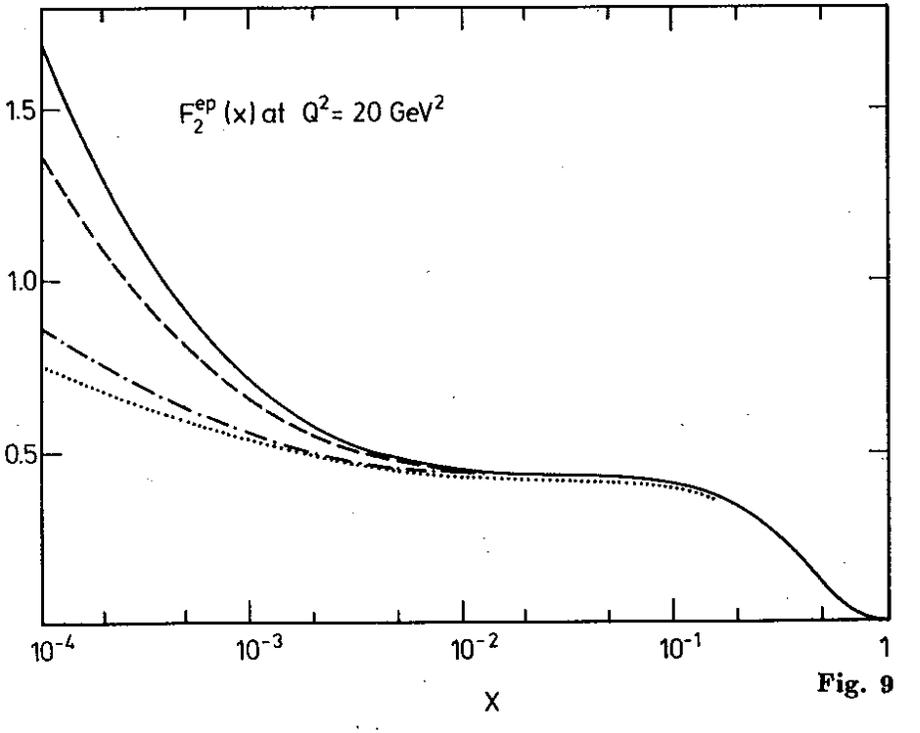

Fig. 9

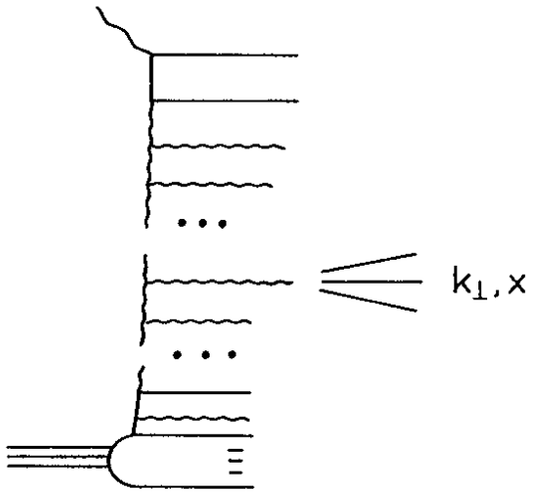

Fig. 10

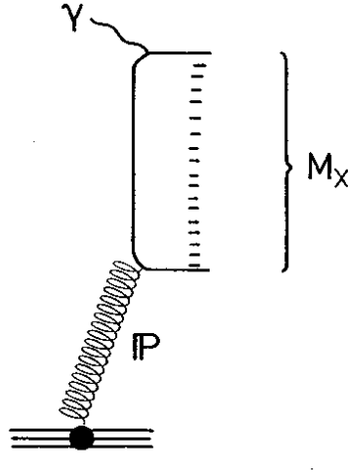

Fig. 11

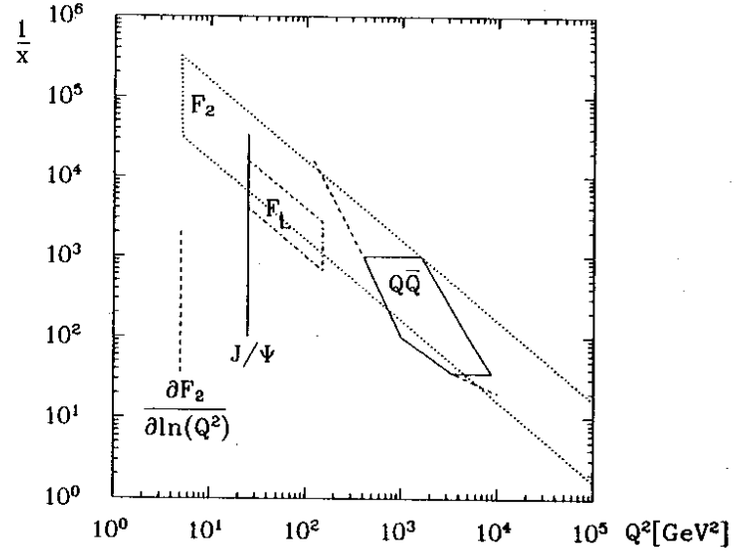

Fig. 12

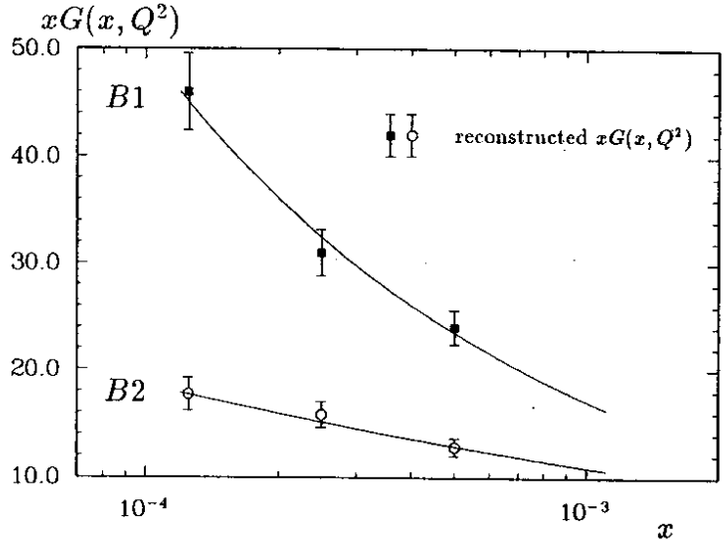

Fig. 13

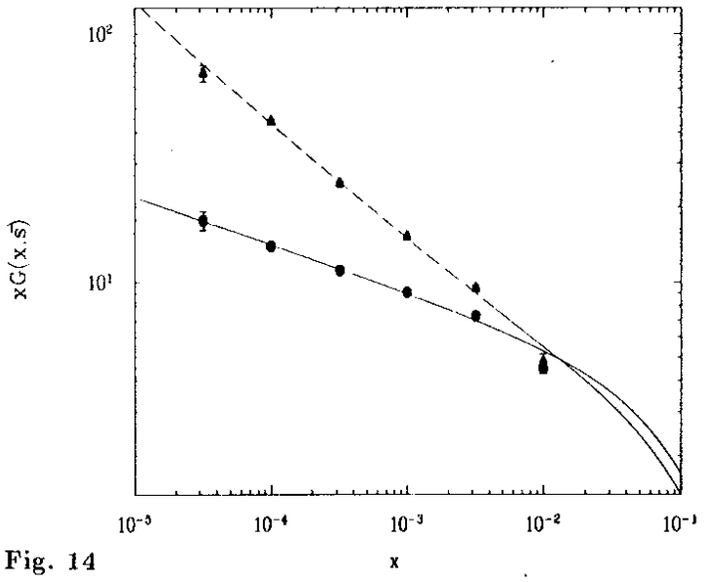
10^2
10^1
$xG(x,s)$
10^{-5}
10^{-4}
10^{-3}
10^{-2}
10^{-1}
x

Fig. 14

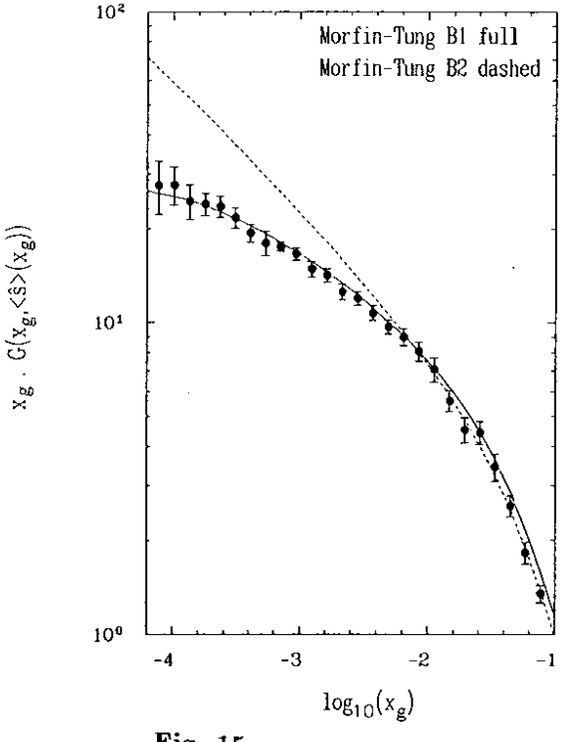
Morfin-Tung B1 full
Morfin-Tung B2 dashed
10^2
10^1
10^0
$x_g \cdot G(x_g,\langle s\rangle(x_g))$
-4
-3
-2
-1
$\log_{10}(x_g)$

Fig. 15